



15 **Abstract.** A new weakly coupled land data assimilation (WCLDA) system based on the four-dimensional  
16 ensemble variational (4D<sub>En</sub>Var) method is developed and applied to the fully coupled Energy Exascale  
17 Earth System Model version 2 (E3SMv2). The dimension-reduced projection four-dimensional  
18 variational (DRP-4D<sub>Var</sub>) method is employed to implement 4D<sub>Var</sub> using the ensemble technique instead  
19 of the adjoint technique. With an interest in providing initial conditions for decadal climate predictions,  
20 monthly mean anomalies of soil moisture and temperature from the Global Land Data Assimilation  
21 System (GLDAS) reanalysis from 1980 to 2016 are assimilated into the land component of E3SMv2  
22 within the coupled modeling framework with a one-month assimilation window. The coupled  
23 assimilation experiment is evaluated using multiple metrics, including the cost function, assimilation  
24 efficiency index, correlation, root mean square error (RMSE) and bias, and compared with a control  
25 simulation without land data assimilation. The WCLDA system yields improved simulation of soil  
26 moisture and temperature compared with the control simulation, with improvements found throughout  
27 the soil layers and in many regions of the global land. In terms of both soil moisture and temperature, the  
28 assimilation experiment outperforms the control simulation with reduced RMSE and higher temporal  
29 correlation in many regions, especially in South America, Central Africa, Australia, and large parts of  
30 Eurasia. Furthermore, significant improvements are also found in reproducing the time evolution of the  
31 2012 U.S. Midwest drought, highlighting the crucial role of land surface in drought lifecycle. The  
32 WCLDA system is intended to be a foundational resource for research to investigate land-derived climate  
33 predictability.

删除了: initial

35 **1 Introduction**

36 The intrinsic chaos of the atmosphere limits traditional weather forecasting to roughly two weeks  
37 (Simmons and Hollingsworth, 2002). The feasibility of atmospheric predictability beyond two weeks lies  
38 with the interactions of the atmosphere with slowly varying components of the Earth system such as the  
39 ocean or land surface, or from predictable external forcings (Guo et al., 2012). Climate prediction can  
40 therefore be conceptually divided into both an initial value and a forced boundary value problem (Collins  
41 and Allen, 2002; Conil et al., 2007). One of the biggest technical challenges for improving the quality of  
42 climate predictions is the initialization of coupled models from observations (Taylor et al., 2012).

43 Much work has been devoted to initializing climate system models for practicable decadal climate  
44 predictions (DCPs). These models couple various components, such as models of the atmosphere, ~~ocean,~~  
45 ~~sea ice, land and river.~~ Due to their complexity, coupled models are often more susceptible to initial  
46 conditions (ICs) than their individual model components, underscoring the importance of ~~data~~  
47 assimilation (DA) (Sakaguchi et al., 2012). The ~~application of~~ DA methods is essential to incorporate  
48 ~~reanalysis data into~~ the components of coupled model and produce the optimal ~~ICs to improve DCPs.~~  
49 ~~The initialization for DCPs uses both~~ uncoupled DA and coupled data assimilation (CDA) methods.  
50 Uncoupled DA performs DA under the framework of an individual component model (e.g., standalone  
51 land surface model forced by atmospheric observations or reanalysis data rather than coupled with an  
52 atmospheric model), and then the uncoupled DA analyses from different individual components are  
53 combined to form the ICs of a coupled model (Zhang et al., 2020). For example, most existing reanalysis  
54 data were produced using uncoupled DA approaches, and these reanalysis datasets are then directly used  
55 to initialize DCPs in some studies (Du et al., 2012; Bellucci et al., 2013). However, such uncoupled DA  
56 often exhibits poor consistency among the ICs of different component models, and eventually produces  
57 low prediction skills (Balmaseda et al., 2009; Boer et al., 2016; Ardilouze et al., 2017).

58 To obtain balanced multi-component ICs in coupled models, recent studies focus on the  
59 development of CDA methods under the coupled modeling framework (Penny and Hamill, 2017; He et  
60 al., 2020a). The purpose of CDA is to produce balanced and coherent ICs for all components within the  
61 climate system by incorporating ~~reanalysis~~ information from one or more components in the coupled  
62 model, providing great potential for improving seamless climate predictions (Dee et al., 2014). Some

删除了： land surface, ocean, sea ice, and so on.

删除了： much higher

删除了： dedicated

删除了： capability

删除了： available observations

删除了： estimate of ICs to improve DCPs.

删除了： observational

70 studies underscore the superior advantages of CDA over traditional uncoupled DA methods (Lea et al.,  
71 2015; Zhang et al., 2005). CDA methods are categorized into two main types: weakly coupled data  
72 assimilation (WCDA) and strongly coupled data assimilation (SCDA). WCDA assimilates the  
73 observations or existing reanalysis into the respective component of the coupled model and then transfers  
74 ~~reanalysis information to the other components through the coupled model integration (He et al., 2020b;~~  
75 ~~Zhang et al., 2020).~~ Considering that sequential DA encompasses both the analysis and the forecast steps,  
76 WCDA allows no direct influence of ~~reanalysis information~~ from a single component to other  
77 components in the analysis step as the cross-component background error covariances are not used, but  
78 coupling in the forecast step allows interactions across different components during the model integration  
79 (Browne et al., 2019) and propagates ~~reanalysis information to other components.~~ In contrast, SCDA  
80 utilizes cross-component background error covariances to directly assimilate ~~reanalysis information from~~  
81 one component into all components, treating the entire Earth system model as one unified system (Penny  
82 et al., 2019). Furthermore, similar to WCDA, SCDA also allows coupling in the forecast step to propagate  
83 ~~reanalysis information from one component to the other components (Yoshida and Kalnay, 2018).~~  
84 Several studies indicate that SCDA typically exhibits more pronounced improvements in assimilation  
85 performance relative to WCDA (Smith et al., 2015; Sluka et al., 2016). However, the application of  
86 SCDA poses substantial technical challenges, particularly in the establishment of effective cross-  
87 component background error covariances. Consequently, the majority of contemporary CDA systems  
88 still utilize the WCDA framework.

89 Recent research efforts have started to implement the CDA system to initialize DCPs, using a  
90 diverse range of DA techniques from simple to complex. The simplest method is nudging which adjusts  
91 the model states towards the observations or existing reanalysis (Hoke and Anthes, 1976; Zhang et al.,  
92 2020). Although the nudging method is time-saving and easy to implement, its application in CDA is  
93 restricted primarily due to the limited types of observations and the required interpolation of observations  
94 at every time step of model integration (He et al., 2017). Previous studies have developed advanced CDA  
95 systems using variational and filtering approaches, such as the three-dimensional variational data  
96 assimilation (3DVar) (Fujii et al., 2009; Yao et al., 2021), and ensemble-based techniques like the  
97 ensemble Kalman filter (EnKF) (Zhang et al., 2007). The former generally utilizes the stationary

删除了: the

删除了: observational

删除了: observations

删除了: the observational

删除了: the observational

删除了:

删除了: the observations

删除了: Laloyaux et al., 2016

106 background error covariance and assimilates observations sequentially (Lin et al., 2017). In contrast, the  
107 latter uses the flow-dependent forecast error covariance and recursively integrates observations into the  
108 model (Lei and Hacker, 2015). Several studies also show encouraging progress in constructing CDA  
109 systems using four-dimensional variational data assimilation (4DVar) method (Smith et al., 2015; Fowler  
110 and Lawless, 2016). The objective of 4DVar is to optimize four-dimensional model states and provide a  
111 compatible temporal trajectory that matches observational records across each assimilation window  
112 (Mochizuki et al., 2016). The 4DVar method is an advanced assimilation technique that exhibits  
113 superiority over other assimilation techniques like nudging and 3DVar in multiple aspects. Initial shocks  
114 that influence prediction skills can be significantly minimized by the 4DVar approach due to the  
115 dynamical consistency between the model and ICs (Sugiura et al., 2008). However, it is difficult to apply  
116 the 4DVar method for CDA systems in the fully coupled model because of the challenge in adjoint  
117 integration of the coupled model and its high computational cost in the analysis step. Finally, to capitalize  
118 on the strengths of both ensemble and variational techniques, recent studies focus on developing new  
119 hybrid data assimilation methods (Wang et al., 2010; Buehner et al., 2018). The hybrid approach utilizes  
120 an ensemble forecast to generate flow-dependent forecast error covariances and presents a way to  
121 perform 4DVar optimization without the need for tangent linear and adjoint models (Lorenc et al., 2015).  
122 However, most studies on CDA have focused on assimilating observations or reanalysis data of ocean,  
123 atmosphere and even sea ice (He et al., 2017; Li et al., 2021; Kimmritz et al., 2018). There have been  
124 relatively few instances of CDA studies assimilating land observations or [land](#) reanalysis data.

125 In this study, we introduce the development of the 4D<sub>En</sub>Var-based weakly coupled land data  
126 assimilation (WCLDA) system for the Energy Exascale Earth System Model version 2 (E3SMv2) (Golaz  
127 et al., 2022). The 4D<sub>En</sub>Var method in this WCLDA system is the dimension-reduced projection 4DVar  
128 (DRP-4DVar; Wang et al., 2010) which utilizes the ensemble technique as an alternative to the adjoint  
129 technique for implementing 4DVar. In this WCLDA system, monthly mean anomalies of soil moisture  
130 and temperature from a global land reanalysis product are assimilated into the land component of a  
131 coupled climate model in the analysis step, and subsequently during the forecast step, the land reanalysis  
132 information incorporated into the ICs of the land component is propagated to the other components (e.g.,  
133 atmosphere and ocean) through the fully coupled model integration and influences the ICs of all

134 components for the next assimilation window. The primary goal of the WCLDA system is intended to be  
135 a foundational resource for exploring predictability of the Earth system by the E3SM community,  
136 specifically focusing on understanding the sources of predictability provided by land versus ocean, with  
137 an initial focus on DCPs. This WCLDA system also provides the groundwork for future actionable  
138 predictions of Earth system variability using E3SM.

139 The objective of this paper is to introduce the implementation of the 4DEnVar-based WCLDA  
140 system for the land component of E3SMv2. In Section 2, we provide an overview of the E3SMv2 model,  
141 describe the 4DEnVar methodology in detail and outline the framework of the 4DEnVar-based WCLDA  
142 system. Preliminary evaluation of the WCLDA system is presented in Section 3. Finally, conclusions are  
143 discussed in Section 4.

144

## 145 **2 Methods**

### 146 **2.1 Model Description**

147 The model used in this study is a relatively new state-of-the-art Earth system model known as  
148 Energy Exascale Earth System Model version 2 (E3SMv2), supported by the U.S. Department of Energy  
149 (DOE) to improve actionable Earth system predictions and projections (Leung et al., 2020). The  
150 atmospheric component is the E3SM Atmosphere Model version 2 (EAMv2), which is built on the  
151 spectral-element atmospheric dynamical core with 72 vertical levels (Dennis et al., 2012; Taylor et al.,  
152 2020). At the standard resolution, EAMv2 is applied on a cubed sphere with a grid spacing of ~100 km  
153 for the dynamics. The ocean component is the Model for Prediction Across Scales-Ocean (MPAS-O),  
154 which applies the underlying spatial discretization to the primitive equations with 60 layers using a z-  
155 star vertical coordinate (Petersen et al., 2018; Reckinger et al., 2015). The sea ice component is MPAS-  
156 SI, which shares the same Voronoi mesh with MPAS-O, with mesh spacing varying between 60km in the  
157 mid-latitudes and 30 km at the equator and poles (Golaz et al., 2022). The land component is the E3SM  
158 Land Model version 2 (ELMv2), which is based on the Community Land Model version 4.5 (CLM4.5)  
159 (Oleson et al. 2013). Simulations are run in a satellite phenology mode with prescribed leaf area index,  
160 and the prescribed vegetation distribution has been updated for better consistency between land use and  
161 changes in plant functional types described by Golaz et al. (2022). The river transport component is the

删除了: major

163 Model for Scale Adaptive River Transport version 2 (MOSARTv2), which provides detailed  
164 representation of riverine hydrologic variables (Li et al., 2013). These five components exchange fluxes  
165 through the top-level coupling driver version 7 (CPL7) (Craig et al., 2012). Further details on the  
166 E3SMv2 model are described in Golaz et al. (2022).

167

## 168 2.2 Datasets

169 Monthly mean soil moisture and soil temperature data in a total of ten soil layers are produced by  
170 the Global Land Data Assimilation System (GLDAS; Rodell et al., 2004). The GLDAS product generates  
171 optimal fields of land surface states and fluxes in near-real time by forcing multiple offline land surface  
172 models with observation-based data fields. These reliable and high-resolution global land surface datasets  
173 from GLDAS are extensively utilized in weather and climate studies, hydrometeorological investigations  
174 and water cycle research (Chen et al., 2021; Zhang et al., 2018). The GLDAS datasets have been available  
175 globally at high spatial resolution since January 1979 and can be accessed through the Goddard Earth  
176 Science Data and Information Service Center. For more consistency with ELMv2, we utilize GLDAS  
177 data produced by CLM. In contrast to decadal timescales, data signals with temporal resolutions shorter  
178 than one month can potentially introduce undesirable noise, which can adversely affect DCPs when high  
179 temporal resolution data are assimilated into the ICs. Moreover, it is very computationally demanding to  
180 assimilate complex actual observations in the initialization for DCPs that requires long-term DA cycles.  
181 Therefore, similar to most existing initialization approaches for DCPs that assimilate reanalysis data, this  
182 study describes the implementation of a data assimilation approach for initializing DCPs by assimilating  
183 monthly mean GLDAS data within the one-month assimilation window.

移动了(插入) [1]

184 Monthly mean surface soil moisture data from the Advanced Microwave Scanning Radiometer  
185 (AMSR) and land surface temperature data from the Moderate Resolution Imaging Spectrometer  
186 (MODIS) are utilized for validation. (1) The AMSR data provides surface soil moisture estimations by  
187 measuring the microwave emission from the Earth's surface (Njoku et al., 2003). The soil moisture data  
188 from AMSR are widely used in scientific research to study surface water cycles, drought conditions and  
189 hydrologic modeling (Du et al., 2019; McCabe et al., 2008). (2) MODIS is an essential instrument  
190 onboard the Terra and Aqua satellite platforms (Remer et al., 2005). The MODIS datasets provide

191 comprehensive global observations describing atmospheric, terrestrial and oceanic conditions, including  
192 land surface temperature, vegetation indices and cloud properties (Justice et al., 2002). The MODIS  
193 products are extensively utilized for monitoring environmental changes and supporting climate change  
194 research (Gao et al., 2015; Mertes et al., 2015).

195 Current initialization techniques are broadly classified into two categories: full-field assimilation  
196 with reanalysis values, and anomaly assimilation with reanalysis anomalies (Hu et al., 2020; Polkova et  
197 al., 2019). The full-field assimilation is commonly performed to reduce the influence of systematic model  
198 biases by replacing the initial model state with the optimal available estimate of the reanalysis state (Volpi  
199 et al., 2017). However, the model trajectory tends to drift away from the observations and revert to the  
200 model's inherent preferred state because of model deficiencies (Smith et al., 2013). This problem is  
201 partially addressed with the anomaly assimilation by assimilating the reanalysis anomalies added to the  
202 model climatology (Carrassi et al., 2014). In this study, we conduct the anomaly assimilation for the  
203 WCLDA system with bias correction applied to GLDAS data before assimilation. For bias correction,  
204 the difference between GLDAS data and its long-term average is calculated as anomalies and then added  
205 to the simulated model climatology.

206

### 207 **2.3 Data Assimilation Scheme**

208 The 4DVar algorithm in this study is based on the DRP-4DVar technique, which is an efficient  
209 pathway for applying 4DVar through using the ensemble method rather than the adjoint technique (Wang  
210 et al., 2010). The DRP-4DVar method generates the optimal estimation in the sample space through  
211 aligning the observations with ensemble samples along the coupled model trajectory (Liu et al., 2011).

212 DRP-4DVar is an economical approach that minimizes the cost function of the standard 4DVar by  
213 using the ensemble technique instead of the adjoint technique (Wang et al., 2010). The background error  
214 covariance matrix  $B$  is estimated using the pure ensemble covariance. The ensemble members originate  
215 from historical or ensemble forecasts. Considering the high computational cost of ensemble forecasts for  
216 the coupled model in our study, we utilize outputs from the pre-industrial control (PI-CTRL) experiment  
217 of E3SMv2 to generate ensemble members. The instantaneous state at the beginning of each month and  
218 the corresponding monthly mean state of this month from the 100-year balanced PI-CTRL simulation

删除了: observed values

删除了: observed anomalies

删除了: observed state

删除了: observed anomalies



223 are used as the samples of initial condition ( $x_i$ ) and forecast samples ( $y_i$ ). The corresponding perturbation  
 224 samples are calculated as  $x'_i = x_i - \bar{x}$  and  $y'_i = y_i - \bar{y}$ , where  $\bar{x}$  and  $\bar{y}$  are the 100-year average  
 225 values of  $x_i$  and  $y_i$  at the same month, respectively. Then,  $m$  pairs of perturbation samples  
 226 ( $x'_1, x'_2, x'_3, \dots, x'_m$ ) and ( $y'_1, y'_2, y'_3, \dots, y'_m$ ) are selected at each DA analysis step according to the  
 227 correlations between  $y'_i$  and the observational innovation  $y'_{obs} = y_{obs} - y_b$ . ensuring that each  $y'$   
 228 sample is selected independently of the other samples in the ensemble. In this study,  $m = 30$ . Then the  
 229 estimation of the background error covariance matrix  $B$  is represented by the formula in Eq. (1), utilizing  
 230 the selected  $x'$  samples. We implement both horizontal and vertical localization to reduce sampling  
 231 errors due to the finite ensemble size and to alleviate the spurious remote influence from distant grid  
 232 points. Our approach to horizontal localization is to apply a distance-dependent weighting function to  
 233 the background error covariance. The vertical localization is employed to limit the influence of reanalysis  
 234 information on specific soil layers. Please refer to Wang et al. (2018) for more detailed descriptions of  
 235 the localization methodology in our study.

删除了： and the independence between  $y'$  samples.

设置了格式： 字体颜色： 文字 1

$$236 \quad \begin{cases} B = bb^T \\ b = \frac{1}{\sqrt{m-1}} \times (x'_1 - x', x'_2 - x', x'_3 - x', \dots, x'_m - x') \\ x' = \frac{1}{m} (x'_1 + x'_2 + x'_3 + \dots + x'_m) \end{cases} \quad (1)$$

删除了： To remove the spurious remote correlations in the  $B$  matrix, the localization approach is applied to optimize the assimilation performance (Wang et al., 2018).

237 According to Wang et al. (2010), DRP-4DVar produces the analysis increment ( $x'_a$ ) by minimizing  
 238 the 4DVar cost function in the incremental form (Courtier et al., 1994):

$$239 \quad \begin{cases} J(x'_a) = \min_{x'} J(x') \\ J(x') = \frac{1}{2} (x')^T B^{-1} x' + \frac{1}{2} (\mathbf{y}' - \mathbf{y}'_{obs})^T (\mathbf{y}' - \mathbf{y}'_{obs}) \end{cases} \quad (2)$$

240 Here  $x' = x - x_b$  represents the increment of model variables relative to the background;  $\mathbf{y}'_{obs} =$   
 241  $r^{-1} y'_{obs} = r^{-1} (y_{obs} - y_b)$  denotes the weighted observational innovation for monthly mean anomalies  
 242 of soil moisture and temperature, and  $R = rr^T$  is the observational error covariance matrix that is  
 243 usually diagonal;  $\mathbf{y}' = r^{-1} y' = r^{-1} (y - y_b)$  is the weighted projection of the increment ( $x'$ ) onto the  
 244 observation space; the superscript  $T$  represents the transpose.

245 To simplify the calculation of the minimization, the increment of model state variables  $x'$  and the  
 246 corresponding weighted observation increment  $\mathbf{y}'$  are projected onto the dimension-reduced sample  
 247 space through the following projection transformations:

252 
$$\begin{cases} x' = P_x \alpha \\ y' = P_y \alpha \end{cases} \quad (3)$$

253 where  $\alpha$  is the  $m$ -dimension column vector containing the weight coefficients  $(\alpha_1, \alpha_2, \alpha_3, \dots, \alpha_m)$ ;  $P_x$   
 254 and  $P_y$  denote the projection matrices that incorporate the initial condition perturbations and the  
 255 corresponding monthly mean samples as follows:

256 
$$\begin{cases} P_x = (x'_1, x'_2, x'_3, \dots, x'_m) \\ P_y = (y'_1, y'_2, y'_3, \dots, y'_m) \end{cases} \quad (4)$$

257 where  $y'_i = r^{-1}y'_i$  ( $i = 1, 2, \dots, m$ ). Then the original 4DVar cost function defined in Eq. (2) is  
 258 transformed into the following new cost function and the analysis can be computed in the sample space  
 259 by minimizing this new cost function:

260 
$$\begin{cases} J(\alpha_a) = \min J(\alpha) \\ J(\alpha) = \frac{1}{2} \alpha^T B_a^{-1} \alpha + \frac{1}{2} (P_y \alpha - y'_{obs})^T (P_y \alpha - y'_{obs}) \\ x_a = x_b + x'_a = x_b + P_x \alpha_a \end{cases} \quad (5)$$

261 The solution to this minimization problem is formulated as:

262 
$$\alpha_a = (B_a^{-1} + P_y^T P_y)^{-1} P_y^T y'_{obs} \quad (6)$$

263 In this study, the DRP-4DVar-based WCLDA system is used to incorporate the land reanalysis data only.

264 The optimal analysis for the land state variables ( $x_a^{lnd}$ ) is obtained by adding the analysis increment  
 265 ( $x_a'^{lnd}$ ) to the background of land ICs ( $x_b^{lnd}$ ), as expressed in Eq. (7):

266 
$$x_a^{lnd} = x_b^{lnd} + x_a'^{lnd} = x_b^{lnd} + P_x (B_a^{-1} + P_y^T P_y)^{-1} P_y^T y'_{obs} \quad (7)$$

267 In the analysis step, only the land state variables are updated to the optimal analysis ( $x_a^{lnd}$ ).  
 268 Subsequently, we proceed with a one-month freely coupled integration of the E3SMv2 model during the  
 269 forecast step. This integration is initialized from the optimal land ICs ( $x_a^{lnd}$ ) along with the background  
 270 fields as the ICs of other components (e.g., atmosphere and ocean). Throughout this one-month free  
 271 integration, the interactions among the model components indirectly enhance the background states of  
 272 these components (e.g., atmosphere and ocean) for the next assimilation window due to the more realistic  
 273 land state variables. Moreover, this coupled integration also contributes to the balance between the ICs  
 274 of different components.

275

#### 276 2.4 4DVar-based WCLDA System

277 The 4DVar-based WCLDA system is developed to assimilate the monthly mean soil moisture and

278 temperature data from the GLDAS analysis dataset into the land component of E3SMv2 using the DRP-  
 279 4DVar method. Two sets of numerical experiments are conducted to evaluate the performance of land  
 280 data assimilation in the WCLDA system. The control simulation (CTRL) is a 37-year freely coupled  
 281 integration driven by observed external forcings (e.g., solar radiation, greenhouse gas and aerosol  
 282 concentrations) from 1980 to 2016. In the freely coupled simulation, the various components of the Earth  
 283 system model, namely the atmosphere, land, river, ocean, and sea ice, interact dynamically without any  
 284 constraints. The observed external forcing mainly acts on the atmospheric component and then influences  
 285 other components (e.g., land surface, ocean, and sea ice) through their coupling with the atmosphere.  
 286 CTRL provides the benchmark for assessing the performance of the WCLDA system. The assimilation  
 287 experiment (Assim) is conducted from 1980 to 2016 based on the WCLDA system in which the GLDAS  
 288 data are assimilated into the land state variables from the first to the tenth layer with a one-month  
 289 assimilation window under the coupled modeling framework. The effectiveness of the WCLDA system  
 290 is evaluated through the comparison between Assim and CTRL. In both Assim and CTRL, the transient-  
 291 historical external forcings are prescribed following the CMIP6 protocol (Eyring et al., 2016).

删除了:

删除了: restraints

292 The flowchart of the 4DVar-based WCLDA system is illustrated in Figure 1. The DRP-4DVar  
 293 method incorporates three inputs: model background, observational innovation and 30 perturbation  
 294 samples. First, the E3SMv2 model is executed for one month, during which state variables such as model  
 295 background ( $x_b$ ), observational operator ( $H$ ) and observational background ( $y_b$ ) are stored. The model  
 296 background ( $x_b$ ) denotes the monthly initial states before assimilation, and the observational operator ( $H$ )  
 297 represents a one-month integration by the coupled model to generate monthly mean model outputs ( $y_b$ ).  
 298 Second, upon completion of the one-month coupled run, the observational innovation ( $y'_{obs}$ ) is determined  
 299 by calculating the differences in soil moisture and temperature between the monthly mean GLDAS data  
 300 ( $y_{obs}$ ) and the model outputs ( $y_b$ ). From the 100-year sample database of the E3SMv2 PI-CTRL  
 301 simulation, 30 samples of monthly mean perturbation ( $y'$ ) are chosen with the highest absolute correlation  
 302 with the observational innovation. The corresponding 30 monthly IC samples ( $x'$ ) are also obtained.  
 303 Finally, the analysis increment is generated in the sample space and the optimal analysis ( $x_a$ ) is calculated  
 304 using the DRP-4DVar algorithm.

上移了 [1]: In contrast to decadal timescales, data signals with temporal resolutions shorter than one month can potentially introduce undesirable noise, which can adversely affect DCPs when high temporal resolution data are assimilated into the ICs. Moreover, it is very computationally demanding to assimilate complex actual observations in the initialization for DCPs that requires long-term DA cycles. Therefore, similar to most existing initialization approaches for DCPs that assimilate reanalysis data, this study describes the implementation of a data assimilation approach for initializing DCPs by assimilating monthly mean GLDAS data within the one-month assimilation window.

删除了: To alleviate spurious correlations, a localization scheme is implemented in the DRP-4DVar-based WCLDA system (Wang et al., 2018).

305 The schematic diagram in Figure 2 outlines the assimilation process of the 4DVar-based WCLDA

323 system in E3SMv2. The incorporation of GLDAS data into the E3SMv2 model consists of the analysis  
324 step and the forecast step. In the analysis step, the differences between monthly mean GLDAS data and  
325 model outputs are calculated and utilized to produce the optimal assimilation analysis at the beginning of  
326 a one-month assimilation window. Subsequently, in the forecast step, this optimal assimilation analysis is  
327 used as the land ICs combined with the background ICs for other components to conduct one-month  
328 forecast using the E3SMv2 model. This forecast generates the backgrounds of all model components for  
329 the next assimilation window. As a result, the forecasted backgrounds for all components are influenced  
330 by the land reanalysis information incorporated into the ICs of the land component. In general, when the  
331 coupled model is used in the forecast step while the optimal assimilation analysis is updated separately  
332 for the respective component, the assimilation approach is identified as WCDA (Penny et al., 2019; Zhang  
333 et al., 2020).

334 The detailed assimilation process mainly consists of three steps within each one-month assimilation  
335 window: 1) the E3SMv2 model is initially executed for one month to generate the simulated monthly  
336 mean soil moisture and temperature ( $y_b^{ind}$ ); 2) the observational innovation ( $y'_{obs}$ ) is obtained through  
337 subtracting the model simulation ( $y_b^{ind}$ ) from the monthly mean observation ( $y_{obs}^{ind}$ ). This innovation is  
338 then applied to formulate the optimal assimilation analysis of land surface ( $x_a^{ind}$ ) at the beginning of the  
339 assimilation window through the DRP-4DVar method; 3) the E3SMv2 model is rewound to the start of  
340 the month and the second one-month model run is executed using the optimal ICs ( $x_a$ ) to generate the  
341 background for the next assimilation window. Due to multi-component interactions during the one-month  
342 freely coupled integration, the land reanalysis information can potentially benefit other components (e.g.,  
343 atmosphere and ocean) in the coupled modeling framework (Li et al., 2021; Shi et al., 2022). To assimilate  
344 the monthly mean GLDAS product, fully coupled integration by the E3SMv2 model is performed twice  
345 within each one-month assimilation window: first to generate the observational innovation by computing  
346 the differences between the GLDAS data and model outputs for analysis, and second to forecast the  
347 backgrounds of all components for the next assimilation window. When the fully coupled model is  
348 executed for the second one-month run, the land reanalysis information is transferred to the other  
349 components through multi-component interactions. This approach is similar to previous studies that  
350 employed the "two-step" scheme in which the land model integration is performed twice within the same

删除了: to

352 month to assimilate the monthly GRACE-based TWS observations (Houborg et al., 2012; Giroto et al.,  
353 2016).

354

## 355 2.5 Evaluation Metrics

356 The reduction rate of the cost function is a significant metric for verifying the effectiveness of the  
357 WCLDA system and evaluating the extent of [reanalysis](#) information assimilated by the coupled model,  
358 which is formulated as:

$$\begin{cases} J_0 = \frac{1}{2}(y_{obs} - y_b)^T R^{-1}(y_{obs} - y_b) \\ J_1 = \frac{1}{2}(y_{obs} - y_a)^T R^{-1}(y_{obs} - y_a) \end{cases} \quad (8)$$

360 where  $J_0$  and  $J_1$  denote the cost function before and after assimilation respectively,  $y_{obs}$  represents the  
361 GLDAS data,  $y_a$  denotes the monthly mean analyses,  $y_b$  is the observation-space background, and  $R$  is  
362 defined as the observation error covariance matrix. [The observation error covariance matrix  \$R\$  can be](#)  
363 [determined statistically by estimating the variance and covariance of the GLDAS data.](#) Negative value  
364 for this metric indicates that [reanalysis](#) information has been correctly incorporated into the model  
365 variables.

366 Following Yin et al. (2014), the assimilation efficiency (AE) index is defined to evaluate the efficiency  
367 of the WCLDA system as follows:

$$368 \quad AE = \frac{RMSE_{Assim}}{RMSE_{CTRL}} - 1 \quad (9)$$

369 In this equation,  $RMSE_{Assim}$  is the root mean square error (RMSE) between [the analysis value from](#)  
370 [Assim](#) and the reference data, while  $RMSE_{CTRL}$  represents the RMSE between CTRL and the reference  
371 data. Negative (positive) AE value indicates improvements (degradations) by the assimilation. In the  
372 following sections, we use the GLDAS data as the main reference data to verify the correctness of the  
373 WCLDA system, but some analyses are also performed using AMSR surface soil moisture and MODIS  
374 land surface temperature as the reference data.

375

## 376 3 Results

### 377 3.1 Evaluation of the cost function

删除了: observational

删除了: observational

删除了: observational

设置了格式: 字体: (默认) Times New Roman

删除了: Assim

382 Figure 3 displays the time series of the monthly reduction rate of the cost function in the 4DEnVar-  
383 based WCLDA system. In the first month, the reduction rate reaches approximately 26.06% in Assim.  
384 Over the subsequent months, Assim maintains the average reduction rate of 7.73% throughout the entire  
385 37-year period. Furthermore, negative reduction rates are observed in 98.65% of the total months,  
386 indicating the effectiveness of the WCLDA system. These results suggest that the WCLDA system is  
387 correctly implemented, with [GLDAS](#) data successfully assimilated into the coupled model.

删除了: the observational

388

### 389 3.2 Evaluation of the AE index

390 The spatial pattern of the AE index for soil moisture at different depths is depicted in Figure 4. The  
391 AE value exhibits negative signal in most areas for total ten soil layers, suggesting the reduction in RMSE  
392 for soil moisture after assimilation. Significant improvements appear over North America, South America,  
393 southern Africa, Europe, and Asia. However, assimilation performance is degraded in the northern part of  
394 Russia and northern Africa. This is consistent with the findings in other studies that assimilation updates  
395 in northern Russia are limited due to the complexities of accurately representing frozen ground and snow  
396 processes in high latitudes (Edwards et al., 2007; Ireson et al., 2013). As surface soil moisture is highly  
397 susceptible to atmospheric conditions, assimilation performance of surface soil moisture is limited by the  
398 accuracy of atmospheric forcing. Furthermore, some degradations found in the deep layers could be  
399 attributed to the substantial influence of various terrestrial factors, such as subsurface runoff and  
400 interactions with groundwater, similar to the findings in previous studies (Liu and Mishra, 2017; Zeng  
401 and Decker, 2009).

402 Figure 5 shows the spatial distribution of the AE index for soil temperature from surface to deep  
403 layers. Most grid cells from the ten soil layers are dominated by negative AE signals, indicating improved  
404 performance for soil temperature after assimilation. Moreover, the spatial patterns across different soil  
405 layers are highly consistent with each other and exhibit similar magnitudes in most areas. Notable  
406 improvements are observed in central Europe, South America, eastern Russia, and large parts of Eurasia  
407 and North America. In contrast, slight degradations appear over Southeast Asia and along the northern  
408 fringes of Africa. This may be partly related to model uncertainties and possible atmospheric noise, as  
409 shown by many past studies (Kwon et al., 2016; Lin et al., 2020).

411 We further perform an analysis of the spatial pattern of the AE index for surface soil moisture and  
412 land surface temperature between satellite data and model simulations (Figure A1). For surface soil  
413 moisture, the comparison with AMSR data suggests that the majority of global regions exhibit reduced  
414 RMSE after assimilation. The reduction of RMSE is pronounced in central North America, South America,  
415 southern Africa, Australia, and Europe. However, in high-latitude areas, significant degradations are  
416 observed in northern Russia, which may be possibly related to model deficiencies in simulating the  
417 complex frozen ground and snow processes (Edwards et al., 2007; Ireson et al., 2013). Regarding land  
418 surface temperature, improved performances are evident over South America, Australia, southern Africa,  
419 and large parts of Eurasia when compared to MODIS data. In contrast, some degradations appear over  
420 parts of North America and central Asia, which still require further improvement.

421

### 422 3.3 Evaluation of the correlation

423 Figure 6 displays the spatial patterns of the differences in temporal correlations for soil moisture  
424 between Assim and CTRL with GLDAS data across different soil layers. The majority of global regions  
425 in Assim exhibit higher correlations from the first to the tenth layer compared with CTRL, suggesting the  
426 overall good performance of the WCLDA system. Enhanced correlations in deep soil layers are more  
427 pronounced than in shallow layers, which may be attributed to the longer memory of soil processes in the  
428 deeper soil layers (Wang et al., 2010). Improved correlations appear over North America, central Europe,  
429 Asia, and parts of Africa. However, some scattered areas show slight degradations, such as northern South  
430 America, central Africa, and eastern Russia. Overall, Assim outperforms CTRL with higher correlation  
431 (Figure 6) and lower RMSE (Figure 4) in many regions, such as Europe, North America, southern South  
432 America, and South Asia.

删除了: observations

433 The correlation differences in soil temperature between Assim and CTRL from surface to deep  
434 layers are shown in Figure 7. Assim yields improved correlations from the first to the tenth layer across  
435 the majority of global regions. Furthermore, similar spatial patterns and magnitudes are observed in the  
436 performance of different soil layers, implying the significant heat transfer from the surface to deep zone  
437 that constrains soil temperature across the soil column. Notable improvements are located over South  
438 America, central Africa, Australia, central Europe, and East Asia. Nevertheless, some degradations

440 appear over North America, western Europe, and Northeast China. Assim shows superior performance  
441 over CTRL for soil temperature with higher correlation (Figure 7) and lower RMSE (Figure 5) in many  
442 regions, including South America, central Europe, Australia, and central Africa.

443

### 444 **3.4 RMSE and bias of the global mean soil moisture and temperature**

445 The vertical distributions of RMSE differences between Assim and CTRL for soil moisture and  
446 temperature are evaluated in Figure 8. Compared with CTRL, Assim shows noticeable improvements  
447 with reduced RMSE for both soil moisture and temperature in all ten soil layers. For soil moisture, the  
448 reduction of RMSE increases with depth from the upper to deep soil layers, reaching its maximum at the  
449 tenth layer. This could be attributed to the longer soil memory in deep layers than shallow layers. For soil  
450 temperature, the reduction of RMSE exhibits similar magnitude from the surface to deep soil layers, which  
451 may be explained by the significant heat transfer across different soil layers in regulating soil temperature  
452 throughout the soil column.

453 Figure 9 shows the time evolutions of the vertically averaged global mean soil moisture and  
454 temperature bias and RMSE differences. For soil moisture bias (Figure 9a), CTRL exhibits dry biases  
455 during the first twenty years and wet biases afterwards. In contrast, Assim shows smaller biases during  
456 both periods by reducing the dry bias prior to ~2000 and the wet bias thereafter. Assim also exhibits  
457 reduced RMSE (Figure 9b) for soil moisture throughout the entire 37-year period. For soil temperature  
458 bias (Figure 9c), CTRL and Assim display comparable performances, possibly due to the small magnitude  
459 of model deviation in soil temperature. The RMSE differences (Figure 9d) suggest that Assim decreases  
460 the RMSE for soil temperature in the majority of months, with 74.10% of the total months in Assim  
461 exhibiting lower RMSE than CTRL. In summary, the superior performance for both soil moisture and  
462 temperature in Assim demonstrates that land reanalysis information has been effectively incorporated into  
463 the model variables through the WCLDA system.

464 Noticeably, the simulated soil temperature and soil moisture display similar long-term trends, with  
465 cold and dry biases before ~2000 and warm and wet biases afterwards. The soil temperature biases may  
466 be related to the global surface air temperature simulated in E3SMv2, which is notably too cold compared  
467 to the observed record during the 1970s and 1980s while the model warms up quickly after ~year 2000



468 (see Figure 23 of Golaz et al., 2022). The global surface air temperature biases during the past decades in  
469 E3SMv1 and v2 have been attributed to the strong aerosol forcing in the model (Golaz et al., 2019; 2022).  
470 As the global mean precipitation scales with the surface temperature at ~2% per degree (Allen and Ingram,  
471 2002), model biases in surface temperature are reflected in biases in precipitation and hence soil moisture,  
472 resulting in similar long-term trends between soil temperature and soil moisture biases in the simulations.  
473

### 474 3.5 2012 U.S. Midwest Drought

475 To further evaluate the performance of the WCLDA system, we briefly investigate the impact of land  
476 data assimilation on simulating the temporal evolution of the U.S. Midwest drought in 2012. Time series  
477 of soil moisture percentiles over the Midwest (36°-50°N, 102°-88°W) demonstrate significant  
478 improvements by Assim in reproducing the time evolution of agricultural drought in 2012 compared with  
479 CTRL (Figure 10). From ERA-Interim data, the agricultural drought starts in August 2011, follows by a  
480 brief relief in early spring of 2012, peaks in September 2012, and recovers by January 2013. The drought  
481 develops rapidly between May and July 2012 over a wide-spread area including the central and  
482 midwestern U.S. This flash drought caused significant agricultural damages and economic losses.

483 The free running CTRL experiment fails to simulate the temporal evolution of the 2012 Midwest  
484 drought, with a correlation coefficient between CTRL and ERA-Interim of only 0.27. The onset and peak  
485 of the drought are remarkably well captured by Assim, although the drought recovery occurs two months  
486 later than observed. The correlation coefficient of the Assim time series with ERA-Interim is 0.56, which  
487 is statistically significant at the 95% confidence level. Our results highlight the importance of land surface  
488 states for drought lifecycle, with the potential to improve future drought predictions through the  
489 implementation of the WCLDA system.

490

### 491 4 Conclusions

492 In this study, we developed the 4DEnVar-based WCLDA system for the E3SMv2 model and  
493 evaluated the performance of this WCLDA system. The DRP-4DVar method was employed for  
494 implementing 4DVar using the ensemble method rather than the adjoint technique. Special attention is  
495 paid to directly assimilating monthly mean land reanalysis data in this system without interpolating to

删除了: the observation based on

删除了: observation

删除了: observation

499 every time step. Within each one-month assimilation window, we assimilate land reanalysis information  
500 into the coupled model without breaking the land-atmosphere interaction, which is important for the  
501 WCLDA system to be used to understand the potential sources of predictability provided by land.

502 ~~Monthly mean anomalies of soil moisture and temperature from the GLDAS reanalysis are~~  
503 ~~assimilated from 1980 to 2016 through the WCLDA system,~~ and its performance is evaluated using  
504 multiple metrics, including the cost function, AE index, correlation, RMSE and bias. Compared with  
505 CTRL, the cost function is reduced by Assim in most months, suggesting that the GLDAS reanalysis data  
506 has been effectively incorporated into the model. In terms of both soil moisture and temperature, Assim  
507 outperforms CTRL with lower RMSE and higher temporal correlation in many regions, especially in  
508 South America, central Africa, Australia, and large parts of Eurasia. For soil moisture bias, Assim further  
509 decreases the dry bias during the first twenty years and the wet bias thereafter. It is noteworthy that the  
510 subseasonal-to-seasonal time evolution of soil moisture percentiles during the 2012 U.S. Midwest drought  
511 can be quite well captured in Assim, underscoring the significant role of land surface states in drought  
512 propagation.

513 Our current WCLDA system has some limitations ~~and requires future improvements. Future~~  
514 ~~enhancements of our WCLDA system will explore the assimilation of additional land products,~~  
515 ~~particularly those derived from satellite observations. The incorporation of such satellite-based datasets~~  
516 ~~is expected to further improve the performance of the WCLDA system.~~ It is possible that the influence of  
517 the WCLDA system on atmospheric processes may be limited in some domains due to uncertainties of  
518 the model parameterizations, particularly in representing land-atmosphere interactions (Zhou et al., 2023).  
519 For example, in humid regions where the evaporation process is predominantly energy-limited, the  
520 assimilation of soil moisture tends to exert limited influence. Instead, the assimilation of soil temperature  
521 may yield more substantial improvements. This underscores the importance of the unique characteristics  
522 and constraints presented by complicated regional conditions in the application of assimilation processes.  
523 To this end, the application of the WCLDA system would motivate future work to better understand the  
524 roles of the land surface in climate variability and provide a foundational resource for future predictability  
525 studies by the E3SM community.

526

删除了： The WCLDA system is conducted from 1980 to 2016

删除了： such as the lack of an observation operator to integrate actual observations (e.g., satellite and station data). An observation operator is crucial in providing the linkage between the model variables and actual observations, which differ in spatial and temporal resolutions. Hence future exploration will focus on developing observation operators suitable for assimilating various satellite data, such as the AMSR-E and GRACE data.

设置了格式： 字体： (中文) Times New Roman, 字体颜色： 自动设置

537 *Code and data availability.* The E3SMv2 source codes used in this study can be accessed on Zenodo at  
538 <https://zenodo.org/record/8194050>. The GLDAS monthly soil moisture and soil temperature data are  
539 available online (<https://disc.gsfc.nasa.gov/datasets?keywords=GLDAS%20monthly&page=1>). The  
540 MODIS monthly land surface temperature data can be downloaded from the website  
541 ([https://disc.gsfc.nasa.gov/datasets/MOD11CM1D\\_005/summary](https://disc.gsfc.nasa.gov/datasets/MOD11CM1D_005/summary)). The AMSR monthly surface soil  
542 moisture data are available from <https://doi.org/10.11888/Soil.tpd.270960>. The ERA-Interim monthly  
543 soil moisture data are available at [https://apps.ecmwf.int/archive-](https://apps.ecmwf.int/archive-catalogue/?levtype=sfc&type=an&class=ei&stream=moda&expver=1)  
544 [catalogue/?levtype=sfc&type=an&class=ei&stream=moda&expver=1](https://apps.ecmwf.int/archive-catalogue/?levtype=sfc&type=an&class=ei&stream=moda&expver=1). The model data used in this study  
545 can be found on Zenodo at <https://zenodo.org/record/8148737>.

546

547 *Author contributions.* LRL initiated this study. PS and LRL designed the experiments. PS developed the  
548 data assimilation code and performed the simulations. BW provided advice on the data assimilation  
549 technique and KZ and SZ provided assistance with the E3SM model. PS and LRL analyzed and  
550 interpreted the data. PS and LRL wrote the paper. BW, KZ, SMH, and SZ contributed to the revision.

551

552 *Competing interests.* The authors declare no competing interests.

553

554 *Acknowledgements.* This research was supported by the Office of Science, Department of Energy  
555 Biological and Environmental Research as part of the Regional and Global Model Analysis program area.  
556 Pacific Northwest National Laboratory is operated by Battelle Memorial Institute for the U.S.  
557 Department of Energy under contract DE-AC05-76RL01830.

558 **References**

- 559 Allen, M. R., and Ingram, W. J.: Constraints on future changes in climate and the hydrologic cycle, *Nature*,  
560 419, 224–232, <https://doi.org/10.1038/nature01092>, 2002.
- 561 Ardilouze, C., Batté, L., Bunzel, F., Decremer, D., Déqué, M., Doblas-Reyes, F. J., Douville, H., Fereday,  
562 D., Guemas, V., MacLachlan, C. and Müller, W.: Multi-model assessment of the impact of soil  
563 moisture initialization on mid-latitude summer predictability, *Climate Dynamics*, 49, 3959–3974,  
564 <https://doi.org/10.1007/s00382-017-3555-7>, 2017.
- 565 Balmaseda, M. A., Alves, O. J., Arribas, A., Awaji, T., Behringer, D. W., Ferry, N., Fujii, Y., Lee, T.,  
566 Rienecker, M., Rosati, T. and Stammer, D.: Ocean initialization for seasonal forecasts,  
567 *Oceanography*, 22(3), 154–159, <https://doi.org/10.5670/oceanog.2009.73>, 2009.
- 568 Bellucci, A., Gualdi, S., Masina, S., Storto, A., Scoccimarro, E., Cagnazzo, C., Fogli, P., Manzini, E., and  
569 Navarra, A.: Decadal climate predictions with a coupled OAGCM initialized with oceanic  
570 reanalyses, *Climate Dynamics*, 40, 1483–1497, <https://doi.org/10.1007/s00382-012-1468-z>, 2013.
- 571 Boer, G. J., Smith, D. M., Cassou, C., Doblas-Reyes, F., Danabasoglu, G., Kirtman, B., Kushnir, Y.,  
572 Kimoto, M., Meehl, G. A., Msadek, R. and Mueller, W. A.: The decadal climate prediction project  
573 (DCPP) contribution to CMIP6, *Geoscientific Model Development*, 9(10), 3751–3777,  
574 <https://doi.org/10.5194/gmd-9-3751-2016>, 2016.
- 575 Browne, P. A., De Rosnay, P., Zuo, H., Bennett, A., and Dawson, A.: Weakly coupled ocean-atmosphere  
576 data assimilation in the ECMWF NWP system, *Remote Sensing*, 11(3), 234,  
577 <https://doi.org/10.3390/rs11030234>, 2019.
- 578 Buehner, M., Du, P., and Bédard, J.: A new approach for estimating the observation impact in ensemble-  
579 variational data assimilation, *Monthly Weather Review*, 146(2), 447–465,  
580 <https://doi.org/10.1175/MWR-D-17-0252.1>, 2018.
- 581 Carrassi, A., Weber, R. J. T., Guemas, V., Doblas-Reyes, F. J., Asif, M., and Volpi, D.: Full-field and  
582 anomaly initialization using a low-order climate model: a comparison and proposals for advanced  
583 formulations, *Nonlinear Processes in Geophysics*, 21, 521–537, [https://doi.org/10.5194/npg-21-521-](https://doi.org/10.5194/npg-21-521-2014)  
584 2014, 2014.
- 585 Chen, Z., Zeng, Y., Shen, G., Xiao, C., Xu, L., and Chen, N. C.: Spatiotemporal characteristics and

586 estimates of extreme precipitation in the Yangtze River Basin using GLDAS data, *International*  
587 *Journal of Climatology*, 41, 1812–1830, <https://doi.org/10.1002/joc.6813>, 2021.

588 Collins, M. and Allen, M. R.: Assessing the relative roles of initial and boundary conditions in interannual  
589 to decadal climate predictability, *Journal of Climate*, 15, 3104–3109, [https://doi.org/10.1175/1520-](https://doi.org/10.1175/1520-0442(2002)015<3104:ATRROI> 2.0.CO;2)  
590 [0442\(2002\)015<3104:ATRROI> 2.0.CO;2](https://doi.org/10.1175/1520-0442(2002)015<3104:ATRROI> 2.0.CO;2), 2002.

591 Conil, S., Douville, H., and Tyteca, S.: The relative influence of soil moisture and SST in climate  
592 predictability explored within ensembles of AMIP type experiments, *Climate Dynamics*, 28, 125–  
593 145, <https://doi.org/10.1007/s00382-006-0172-2>, 2007.

594 Courtier, P., Thépaut, J. M., and Hollingsworth, A.: A strategy for operational implementation of 4D-Var,  
595 using an incremental approach, *Quarterly Journal of the Royal Meteorological Society*, 120, 1367–  
596 1387, <https://doi.org/10.1002/qj.49712051912>, 1994.

597 Craig, A. P., Vertenstein, M., and Jacob, R.: A new flexible coupler for Earth system modeling developed  
598 for CCSM4 and CESM1, *International Journal of High Performance Computing Applications*, 26(1),  
599 31–42, <https://doi.org/10.1177/1094342011428141>, 2012.

600 Dee, D. P., Balmaseda, M., Balsamo, G., Engelen, R., Simmons, A. J., and Thépaut, J. N.: Toward a  
601 consistent reanalysis of the climate system, *Bulletin of the American Meteorological Society*, 95(8),  
602 1235–1248, <https://doi.org/10.1175/BAMS-D-13-00043.1>, 2014.

603 Dennis, J. M., Edwards, J., Loy, R., Jacob, R., Mirin, A. A., Craig, A. P., and Vertenstein, M.: An  
604 application-level parallel I/O library for Earth system models, *International Journal of High*  
605 *Performance Computing Applications*, 26(1), 43–53, <https://doi.org/10.1177/1094342011428143>,  
606 2012.

607 Du, H., Doblas-Reyes, F. J., Garcia-Serrano, J., Guemas, V., Soufflet, Y., and Wouters, B.: Sensitivity of  
608 decadal predictions to the initial atmospheric and oceanic perturbations, *Climate Dynamics*, 39(7),  
609 2013–2023, <https://doi.org/10.1007/s00382-011-1285-9>, 2012.

610 [Du, J., Kimball, J. S., Velicogna, I., Zhao, M., Jones, L. A., Watts, J. D., and Kim, Y.: Multicomponent](https://doi.org/10.1029/2018WR024633)  
611 [satellite assessment of drought severity in the contiguous United States from 2002 to 2017 using](https://doi.org/10.1029/2018WR024633)  
612 [AMSR-E and AMSR2, \*Water Resources Research\*, 55\(7\), 5394–5412,](https://doi.org/10.1029/2018WR024633)  
613 <https://doi.org/10.1029/2018WR024633>, 2019.

614 Edwards, A. C., Scalenghe, R., and Freppaz, M.: Changes in the seasonal snow cover of alpine regions  
615 and its effect on soil processes: a review, *Quaternary International*, 162, 172–181,  
616 <https://doi.org/10.1016/j.quaint.2006.10.027>, 2007.

617 Eyring, V., Bony, S., Meehl, G. A., Senior, C. A., Stevens, B., Stouffer, R. J., and Taylor, K. E.: Overview  
618 of the Coupled Model Intercomparison Project Phase 6 (CMIP6) experimental design and  
619 organization, *Geoscientific Model Development*, 9, 1937–1958, [https://doi.org/10.5194/gmd-9-](https://doi.org/10.5194/gmd-9-1937-2016)  
620 1937-2016, 2016.

621 Fowler, A. M., and Lawless, A. S.: An idealized study of coupled atmosphere–ocean 4D-Var in the  
622 presence of model error, *Monthly Weather Review*, 144(10), 4007–4030,  
623 <https://doi.org/10.1175/MWR-D-15-0420.1>, 2016.

624 [Fujii, Y., Nakaegawa, T., Matsumoto, S., Yasuda, T., Yamanaka, G., and Kamachi, M.: Coupled climate  
625 simulation by constraining ocean fields in a coupled model with ocean data, \*Journal of Climate\*, 22,  
626 5541–5557, <https://doi.org/10.1175/2009JCLI2814.1>, 2009.](#)

627 [Gao, F., Hilker, T., Zhu, X., Anderson, M., Masek, J., Wang, P., and Yang, Y.: Fusing Landsat and MODIS  
628 data for vegetation monitoring, \*IEEE Geoscience and Remote Sensing Magazine\*, 3\(3\), 47–60,  
629 <https://doi.org/10.1109/MGRS.2015.2434351>, 2015.](#)

630 Girotto, M., De Lannoy, G. J., Reichle, R. H., and Rodell, M.: Assimilation of gridded terrestrial water  
631 storage observations from GRACE into a land surface model, *Water Resources Research*, 52(5),  
632 4164–4183, <https://doi.org/10.1002/2015WR018417>, 2016.

633 Golaz, J. C., Caldwell, P. M., Van Roekel, L. P., Petersen, M. R., Tang, Q., Wolfe, J. D., Abeshu, G.,  
634 Anantharaj, V., Asay-Davis, X. S., Bader, D. C., Baldwin, S. A., Bisht, G., Bogenschutz, P. A.,  
635 Branstetter, M., Brunke, M. A., Brus, S. R., Burrows, S. M., Cameron-Smith, P. J., Donahue, A. S.,  
636 Deakin, M., Easter, R. C., Evans, K. J., Feng, Y., Flanner, M., Foucar, J. G., Fyke, J. G., Griffin, B.  
637 M., Hannay, C., Harrop, B. E., Hoffman, M. J., Hunke, E. C., Jacob, R. L., Jacobsen, D. W., Jeffery,  
638 N., Jones, P. W., Keen, N. D., Klein, S. A., Larson, V. E., Leung, L. R., Li, H. Y., Lin, W., Lipscomb,  
639 W. H., Ma, P. L., Mahajan, S., Maltrud, M. E., Mamatjanov, A., McClean, J. L., McCoy, R. B.,  
640 Neale, R. B., Price, S. F., Qian, Y., Rasch, P. J., Reeves Eyre, J. E. J., Riley, W. J., Ringler, T. D.,  
641 Roberts, A. F., Roesler, E. L., Salinger, A. G., Shaheen, Z., Shi, X., Singh, B., Tang, J., Taylor, M.

删除了: ↩

643 A., Thornton, P. E., Turner, A. K., Veneziani, M., Wan, H., Wang, H., Wang, S., Williams, D. N.,  
644 Wolfram, P. J., Worley, P. H., Xie, S., Yang, Y., Yoon, J.-H., Zelinka, M. D., Zender, C. S., Zeng, X.,  
645 Zhang, C., Zhang, K., Zhang, Y., Zheng, X., Zhou, T., and Zhu, Q.: The DOE E3SM Coupled Model  
646 Version 1: Overview and Evaluation at Standard Resolution, *Journal of Advances in Modeling Earth  
647 Systems*, 11, 2089–2129, <https://doi.org/https://doi.org/10.1029/2018MS001603>, 2019.

648 Golaz, J. C., Van Roekel, L. P., Zheng, X., Roberts, A. F., Wolfe, J. D., Lin, W. Y., Bradley, A. M., Tang,  
649 Q., Maltrud, M. E., Forsyth, R. M., Zhang, C. Z., Zhou, T., Zhang, K., Zender, C. S., Wu, M. X.,  
650 Wang, H. L., Turner, A. K., Singh, B., Richter, J. H., Qin, Y., Petersen, M. R., Mamatjanov, A., Ma,  
651 P., Larson, V. E., Krishna, J., Keen, N. D., Jeffery, N., Hunke, E. C., Hannah, W. M., Guba, O.,  
652 Griffin, B. M., Feng, Y., Engwirda, D., Vittorio, A. V., Cheng, D., Conlon, L. M., Chen, C., Brunke,  
653 M. A., Bisht, G., Benedict, J. J., Asay-Davis, X. S., Zhang, Y. Y., Zhang, M., Zeng, X. B., Xie, S.  
654 C., Wolfram, P. J., Vo, T., Veneziani, M., Tesfa, T. K., Sreepathi, S., Salinger, A. G., Jack Reeves  
655 Eyre, J. E., Prather, M. J., Mahajan, S., Li, Q., Jones, P. W., Jacob, R. L., Huebler, G. W., Huang, X.  
656 L., Hillman, B. R., Harrop, B. E., Foucar, J. G., Fang, Y. L., Comeau, D. S., Caldwell, P. M.,  
657 Bartoletti, T., Balaguru, K., Taylor, M. A., McCoy, R. B., Leung, L. R., and Bader, D. C.: The DOE  
658 E3SM Model version 2: Overview of the physical model and initial model evaluation, *Journal of  
659 Advances in Modeling Earth Systems*, 14, e2022MS003156, [https://doi.  
660 org/10.1029/2022MS003156](https://doi.org/10.1029/2022MS003156), 2022.

661 Guo, Z., Dirmeyer, P. A., Delsole, T., and Koster, R. D.: Rebound in atmospheric predictability and the  
662 role of the land surface, *Journal of Climate*, 25(13), 4744–4749, [https://doi.org/10.1175/JCLI-D-11-  
00651.1](https://doi.org/10.1175/JCLI-D-11-<br/>663 00651.1), 2012.

664 He, Y., Wang, B., Liu, M., Liu, L., Yu, Y., Liu, J., Li, R., Zhang, C., Xu, S., Huang, W., Liu, Q., Wang,  
665 Y., and Li, F.: Reduction of initial shock in decadal predictions using a new initialization strategy,  
666 *Geophysical Research Letters*, 44(16), 8538–8547, <https://doi.org/10.1002/2017GL074028>, 2017.

667 He, Y., Wang, B., Liu, L., Huang, W., Xu, S., Liu, J., Wang, Y., Li, L., Huang, X., Peng, Y., Lin, Y., and  
668 Yu, Y.: A DRP-4DVar-based coupled data assimilation system with a simplified off-line localization  
669 technique for decadal predictions, *Journal of Advances in Modeling Earth Systems*, 12(4),  
670 e2019MS001768, <https://doi.org/10.1029/2019MS001768>, 2020a.

671 He, Y., Wang, B., Huang, W., Xu, S., Wang, Y., Liu, L., Li, L., Liu, J., Yu, Y., Lin, Y., Huang, X., and  
672 Peng, Y.: A new DRP-4DVar-based coupled data assimilation system for decadal predictions using  
673 a fast online localization technique, *Climate Dynamics*, 54, 3541–3559,  
674 <https://doi.org/10.1007/s00382-020-05190-w>, 2020b.

675 Hoke, J. E. and Anthes, R. A.: The initialization of numerical models by a dynamic-initialization  
676 technique, *Monthly Weather Review*, 104(12), 1551–1556, [https://doi.org/10.1175/1520-0493\(1976\)104<1551:TIONMB>2.0.CO;2](https://doi.org/10.1175/1520-0493(1976)104<1551:TIONMB>2.0.CO;2), 1976.

678 Houborg, R., Rodell, M., Li, B., Reichle, R., and Zaitchik, B. F.: Drought indicators based on model-  
679 assimilated Gravity Recovery and Climate Experiment (GRACE) terrestrial water storage  
680 observations, *Water Resources Research*, 48, W07525, <https://doi.org/10.1029/2011WR011291>,  
681 2012.

682 Hu, S., Zhou, T., and Wu, B.: Improved ENSO prediction skill resulting from reduced climate drift in  
683 IAP-DecPreS: A comparison of full-field and anomaly initializations, *Journal of Advances in*  
684 *Modeling Earth Systems*, 12, e2019MS001759, <https://doi.org/10.1029/2019MS001759>, 2020.

685 Ireson, A. M., Van Der Kamp, G., Ferguson, G., Nachshon, U., and Wheater, H. S.: Hydrogeological  
686 processes in seasonally frozen northern latitudes: understanding, gaps and challenges,  
687 *Hydrogeology Journal*, 21, 53–66, <https://doi.org/10.1007/s10040-012-0916-5>, 2013.

688 [Justice, C. O., Townshend, J. R. G., Vermote, E. F., Masuoka, E., Wolfe, R. E., Saleous, N., Roy, D. P.,](#)  
689 [and Morisette, J. T.: An overview of MODIS Land data processing and product status, \*Remote\*](#)  
690 [Sensing of Environment](#), 83, 3–15, [https://doi.org/10.1016/S0034-4257\(02\)00084-6](https://doi.org/10.1016/S0034-4257(02)00084-6), 2002.

691 [Kimmritz, M., Counillon, F., Bitz, C. M., Massonnet, F., Bethke, I., and Gao, Y.: Optimising assimilation](#)  
692 [of sea ice concentration in an Earth system model with a multicategory sea ice model, \*Tellus\*, 70A,](#)  
693 [1435945, https://doi.org/10.1080/16000870.2018.1435945](#), 2018.

694 [Kwon, Y., Yang, Z. L., Zhao, L., Hoar, T. J., Toure, A. M., and Rodell, M.: Estimating snow water storage](#)  
695 [in North America using CLM4, DART, and snow radiance data assimilation, \*Journal of\*](#)  
696 [Hydrometeorology](#), 17(11), 2853–2874, <https://doi.org/10.1175/JHM-D-16-0028.1>, 2016.

697 [Lea, D. J., Mirouze, I., Martin, M. J., King, R. R., Hines, A., Walters, D., and Thurlow, M.: Assessing a](#)  
698 [new coupled data assimilation system based on the Met Office coupled atmosphere–land–ocean–](#)

删除了: ↵

删除了: Laloyaux, P., Balmaseda, M., Dee, D., Mogensen, K., and Janssen, P.: A coupled data assimilation system for climate reanalysis, *Quarterly Journal of the Royal Meteorological Society*, 142(694), 65-78, <https://doi.org/10.1002/qj.2629>, 2016.↵



705 sea ice model, *Monthly Weather Review*, 143(11), 4678-4694, <https://doi.org/10.1175/MWR-D-15->  
706 0174.1, 2015.

707 Lei, L. L. and Hacker, J. P.: Nudging, ensemble, and nudging ensembles for data assimilation in the  
708 presence of model error, *Monthly Weather Review*, 143(7), 2600–2610,  
709 <https://doi.org/10.1175/MWR-D-14-00295.1>, 2015.

710 Leung, L. R., Bader, D. C., Taylor, M. A., and McCoy, R. B.: An introduction to the E3SM special  
711 collection: Goals, science drivers, development, and analysis, *Journal of Advances in Modeling*  
712 *Earth Systems*, 12(11), e2019MS001821, <https://doi.org/10.1029/2019MS001821>, 2020.

713 Li, F., Wang, B., He, Y., Huang, W., Xu, S., Liu, L., Liu, J. and Li, L.: Important role of North Atlantic  
714 air–sea coupling in the interannual predictability of summer precipitation over the eastern Tibetan  
715 Plateau, *Climate Dynamics*, 56, 1433–1448, <https://doi.org/10.1007/s00382-020-05542-6>, 2021.

716 Li, H. Y., Wigmosta, M. S., Wu, H., Huang, M., Ke, Y., Coleman, A. M., and Leung, L. R.: A physically  
717 based runoff routing model for land surface and Earth system models, *Journal of Hydrometeorology*,  
718 14, 808–828, <https://doi.org/10.1175/JHM-D-12-015.1>, 2013.

719 Lin, L. F., Ebtehaj, A. M., Wang, J., and Bras, R. L.: Soil moisture background error covariance and data  
720 assimilation in a coupled land-atmosphere model, *Water Resources Research*, 53(2), 1309–1335,  
721 <https://doi.org/10.1002/2015WR017548>, 2017.

722 Lin, P., Yang, Z. L., Wei, J., Dickinson, R. E., Zhang, Y., and Zhao, L.: Assimilating multi-satellite snow  
723 data in ungauged Eurasia improves the simulation accuracy of Asian monsoon seasonal anomalies,  
724 *Environmental Research Letters*, 15(6), 064033, <https://doi.org/10.1088/1748-9326/ab80ef>, 2020.

725 Liu, D., and Mishra, A. K.: Performance of AMSR\_E soil moisture data assimilation in CLM4. 5 model  
726 for monitoring hydrologic fluxes at global scale, *Journal of Hydrometeorology*, 547, 67–79,  
727 <https://doi.org/10.1016/j.jhydrol.2017.01.036>, 2017.

728 Liu, J. J., Wang, B., and Xiao, Q. N.: An evaluation study of the DRP-4-DVar approach with the Lorenz-  
729 96 model, *Tellus A: Dynamic Meteorology and Oceanography*, 63, 256–262,  
730 <https://doi.org/10.1111/j.1600-0870.2010.00487.x>, 2011.

731 Lorenc, A. C., Bowler, N. E., Clayton, A. M., Pring, S. R., and Fairbairn, D.: Comparison of hybrid-  
732 4DEnVar and hybrid-4DVar data assimilation methods for global NWP, *Monthly Weather Review*,

733 143, 212–229, <https://doi.org/10.1175/MWR-D-14-00195.1>, 2015.

734 [McCabe, M. F., Wood, E. F., Wójcik, R., Pan, M., Sheffield, J., Gao, H., and Su, H.: Hydrological](#)  
735 [consistency using multi-sensor remote sensing data for water and energy cycle studies, \*Remote\*](#)  
736 [Sensing of Environment](#), 112(2), 430–444, <https://doi.org/10.1016/j.rse.2007.03.027>, 2008.

737 [Mertes, C. M., Schneider, A., Sulla-Menashe, D., Tatem, A. J., and Tan, B.: Detecting change in urban](#)  
738 [areas at continental scales with MODIS data, \*Remote Sensing of Environment\*](#), 158, 331–347,  
739 <https://doi.org/10.1016/j.rse.2014.09.023>, 2015.

740 Mochizuki, T., Masuda, S., Ishikawa, Y., and Awaji, T.: Multiyear climate prediction with initialization  
741 based on 4D-Var data assimilation, *Geophysical Research Letters*, 43(8), 3903–3910,  
742 <https://doi.org/10.1002/2016GL067895>, 2016.

743 [Njoku, E. G., Jackson, T. J., Lakshmi, V., Chan, T. K., and Nghiem, S. V.: Soil moisture retrieval from](#)  
744 [AMSR-E, \*IEEE Transactions on Geoscience and Remote Sensing\*](#), 41(2), 215–229,  
745 <https://doi.org/10.1109/TGRS.2002.808243>, 2003.

746 Oleson, K. W., Lawrence, D. M., Bonan, G. B., Drewniak, B., Huang, M., Koven, C. D., Levis, S., Li,  
747 F., Riley, W. J., Subin, Z. M., Swenson, S. C., Thornton, P. E., Bozbiyik, A., Fisher, R., Heald, C.  
748 L., Kluzek, E., Lamarque, J. F., Lawrence, P. J., Leung, L. R., Lipscomb, W., Muszala, S., Ricciuto,  
749 D. M., Sacks, W., Sun, Y., Tang, J., and Yang, Z. L.: Technical description of version 4.5 of the  
750 Community Land Model (CLM) (Tech. Rep. NCAR/TN-503+STR). Boulder, Colorado, USA:  
751 National Center for Atmospheric Research, <http://dx.doi.org/10.5065/D6RR1W7M>, 2013.

752 Penny, S. G., and Hamill, T. M.: Coupled data assimilation for integrated earth system analysis and  
753 prediction, *Bulletin of the American Meteorological Society*, 98(7), ES169-ES172,  
754 <https://doi.org/10.1175/BAMS-D-17-0036.1>, 2017.

755 Penny, S. G., Bach, E., Bhargava, K., Chang, C. C., Da, C., Sun, L., and Yoshida, T.: Strongly coupled  
756 data assimilation in multiscale media: Experiments using a quasi-geostrophic coupled model,  
757 *Journal of Advances in Modeling Earth Systems*, 11(6), 1803-1829,  
758 <https://doi.org/10.1029/2019MS001652>, 2019.

759 Petersen, M., Asay-Davis, X. S., Jacobsen, D., Maltrud, M., Ringler, T., Van Roekel, L., and Wolfram,  
760 P.: MPAS ocean user's guide V6, Zenodo, <https://doi.org/10.5281/zenodo.1246893>, 2018.

761 Polkova, I., Köhl, A., and Stammer, D.: Climate-mode initialization for decadal climate predictions,  
762 *Climate Dynamics*, 53, 7097–7111, <https://doi.org/10.1007/s00382-019-04975-y>, 2019.

763 Reckinger, S. M., Petersen, M. R., and Reckinger, S. J.: A study of overflow simulations using MPAS-  
764 Ocean: Vertical grids, resolution, and viscosity, *Ocean Modeling*, 96, 291–313,  
765 <https://doi.org/10.1016/j.ocemod.2015.09.006>, 2015.

766 [Remer, L. A., Kaufman, Y. J., Tanré, D., Mattoo, S., Chu, D. A., Martins, J. V., Li, R. R., Ichoku, C.,  
767 Levy, R. C., Kleidman, R. G., Eck, T. F., Vermote, E., and Holben, B. N.: The MODIS aerosol  
768 algorithm, products, and validation, \*Journal of the Atmospheric Sciences\*, 62\(4\), 947–973,  
769 <https://doi.org/10.1175/JAS3385.1>, 2005.](#)

770 Rodell, M., Houser, P. R., Jambor, U., Gottschalck, J., Mitchell, K., Meng, C. J., Arsenault, K., Cosgrove,  
771 B., Radakovich, J., Bosilovich, M. and Entin, J. K., Walker, J. P., Lohmann, D., and Toll, D.: The  
772 global land data assimilation system, *Bulletin of the American Meteorological society*, 85(3), 381–  
773 394, <https://doi.org/10.1175/BAMS-85-3-381>, 2004.

774 Sakaguchi, K., Zeng, X., and Brunke, M. A.: The hindcast skill of the CMIP ensembles for the surface  
775 air temperature trend, *Journal of Geophysical Research: Atmospheres*, 117, D1611,  
776 <https://doi.org/10.1029/2012JD017765>, 2012.

777 Shi, P. F., Wang, B., He, Y., Lu, H., Yang, K., Xu, S. M., Huang, W. Y., Liu, L., Liu, J. J., Li, L. J., and  
778 Wang, Y.: Contributions of weakly coupled data assimilation–based land initialization to interannual  
779 predictability of summer climate over Europe, *Journal of Climate*, 35, 517–535,  
780 <https://doi.org/10.1175/JCLI-D-20-0506.1>, 2022.

781 Simmons, A. J. and Hollingsworth, A.: Some aspects of the improvement in skill of numerical weather  
782 prediction, *Quarterly Journal of the Royal Meteorological Society*, 128(580), 647–677,  
783 <https://doi.org/10.1256/003590002321042135>, 2002.

784 Sluka, T. C., Penny, S. G., Kalnay, E., and Miyoshi, T.: Assimilating atmospheric observations into the  
785 ocean using strongly coupled ensemble data assimilation, *Geophysical Research Letters*, 43(2), 752-  
786 759, <https://doi.org/10.1002/2015GL067238>, 2016.

787 Smith, P. J., Fowler, A. M., and Lawless, A. S.: Exploring strategies for coupled 4DVar data assimilation  
788 using an idealised atmosphere–ocean model, *Tellus A*, 67(1):27025,

789 <https://doi.org/10.3402/tellusa.v67.27025>, 2015.

790 Smith, D. M., Eade, R., and Pohlmann, H.: A comparison of full-field and anomaly initialization for  
791 seasonal to decadal climate prediction, *Climate Dynamics*, 41, 3325–3338,  
792 <https://doi.org/10.1007/s00382-013-1683-2>, 2013.

793 Sugiura, N., Awaji, T., Masuda, S., Mochizuki, T., Toyoda, T., Miyama, T., Igarashi, H. and Ishikawa, Y.:  
794 Development of a four-dimensional variational coupled data assimilation system for enhanced  
795 analysis and prediction of seasonal to interannual climate variations, *Journal of Geophysical*  
796 *Research: Oceans*, 113, C10017, <https://doi.org/10.1029/2008JC004741>, 2008.

797 Taylor, K. E., Stouffer, R. J., and Meehl, G. A.: An overview of CMIP5 and the experiment design,  
798 *Bulletin of the American Meteorological Society*, 93(4), 485–498, [https://doi.org/10.1175/BAMS-](https://doi.org/10.1175/BAMS-D-11-00094.1)  
799 [D-11-00094.1](https://doi.org/10.1175/BAMS-D-11-00094.1), 2012.

800 Taylor, M. A., Guba, O., Steyer, A., Ullrich, P. A., Hall, D. M., and Eldrid, C.: An energy consistent  
801 discretization of the nonhydrostatic equations in primitive variables, *Journal of Advances in*  
802 *Modeling Earth Systems*, 12, e2019MS001783, <https://doi.org/10.1029/2019MS001783>, 2020.

803 Volpi, D., Guemas, V., and Doblas-Reyes, F. J.: Comparison of full field and anomaly initialisation for  
804 decadal climate prediction: towards an optimal consistency between the ocean and sea-ice anomaly  
805 initialisation state, *Climate Dynamics*, 49, 1181–1195, <https://doi.org/10.1007/s00382-016-3373-3>,  
806 2017.

807 Wang, B., Liu, J., Wang, S., Cheng, W., Liu, J., Liu, C., Xiao, Q., and Kuo, Y. H.: An economical approach  
808 to four-dimensional variational data assimilation, *Advances in Atmospheric Sciences*, 27, 715–727,  
809 <https://doi.org/10.1007/s00376-009-9122-3>, 2010.

810 Wang, B., Liu, J., Liu, L., Xu, S., and Huang, W.: An approach to localization for ensemble-based data  
811 assimilation, *PloS one*, 13(1), e0191088, <https://doi.org/10.1371/journal.pone.0191088>, 2018.

812 Wang, G., Dolman, A. J., Blender, R., and Fraedrich, K.: Fluctuation regimes of soil moisture in ERA-  
813 40 reanalysis data, *Theoretical and Applied Climatology*, 99, 1–8, [https://doi.org/10.1007/s00704-](https://doi.org/10.1007/s00704-009-0111-3)  
814 [009-0111-3](https://doi.org/10.1007/s00704-009-0111-3), 2010.

815 Yao, Y., Luo, Y., Huang, J., and Ma, J.: Improving the downscaled springtime temperature in Central  
816 Asia through assimilating meteorological and snow cover observations, *Atmospheric Research*, 258,

817 105619, <https://doi.org/10.1016/j.atmosres.2021.105619>, 2021.

818 Yin, J., Zhan, X., Zheng, Y., Liu, J., Hain, C. R., and Fang, L.: Impact of quality control of satellite soil  
819 moisture data on their assimilation into land surface model, *Geophysical Research Letters*, 41(20),  
820 7159–7166, <https://doi.org/10.1002/2014GL060659>, 2014.

821 Yoshida, T., and Kalnay, E.: Correlation-cutoff method for covariance localization in strongly coupled  
822 data assimilation, *Monthly Weather Review*, 146(9), 2881-2889, [https://doi.org/10.1175/MWR-D-](https://doi.org/10.1175/MWR-D-17-0365.1)  
823 17-0365.1, 2018.

824 Zeng, X., and Decker, M.: Improving the numerical solution of soil moisture-based Richards equation  
825 for land models with a deep or shallow water table, *Journal of Hydrometeorology*, 10, 308–319,  
826 <https://doi.org/10.1175/2008JHM1011.1>, 2009.

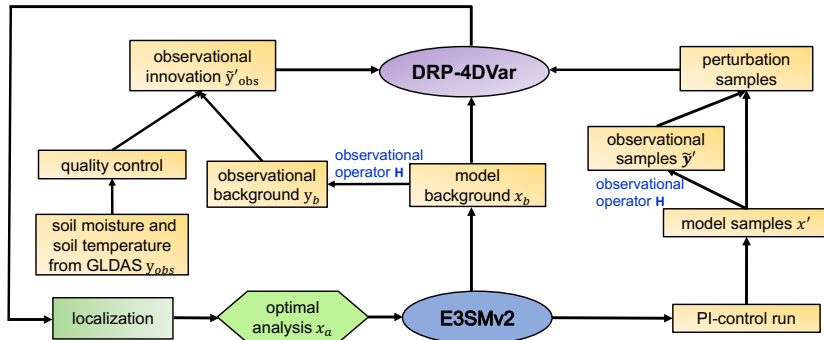
827 Zhang, H., Zhang, L. L., Li, J., An, R. D., Deng, Y.: Climate and Hydrological Change Characteristics  
828 and Applicability of GLDAS Data in the Yarlung Zangbo River Basin, China, *Water*, 10, 254,  
829 <https://doi.org/10.3390/w10030254>, 2018.

830 Zhang, S., Harrison, M. J., Wittenberg, A. T., Rosati, A., Anderson, J. L., and Balaji, V.: Initialization of  
831 an ENSO forecast system using a parallelized ensemble filter, *Monthly Weather Review*, 133(11),  
832 3176-3201, <https://doi.org/10.1175/MWR3024.1>, 2005.

833 Zhang, S., Harrison, M. J., Rosati, A., and Wittenberg, A.: System design and evaluation of coupled  
834 ensemble data assimilation for global oceanic climate studies, *Monthly Weather Review*, 135(10),  
835 3541-3564, <https://doi.org/10.1175/MWR3466.1>, 2007.

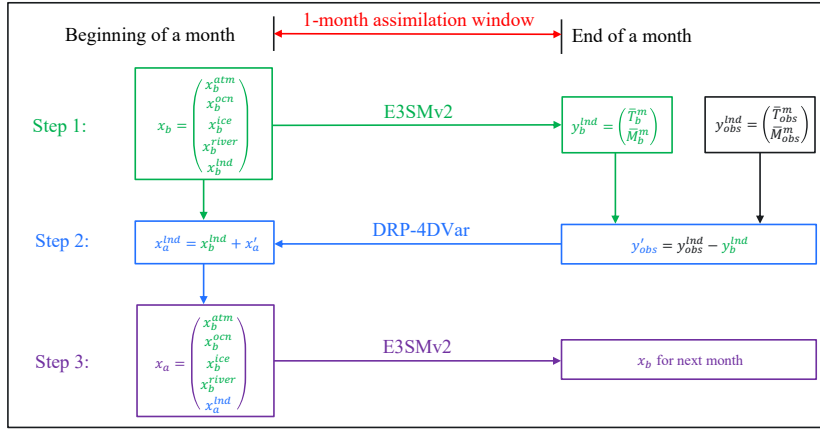
836 Zhang, S., Liu, Z., Zhang, X., Wu, X., Han, G., Zhao, Y., Yu, X., Liu, C., Liu, Y., Wu, S., Lu, F., Li, M.,  
837 Deng, X.: Coupled data assimilation and parameter estimation in coupled ocean-atmosphere models:  
838 a review, *Climate Dynamics*, 54, 5127-5144, <https://doi.org/10.1007/s00382-020-05275-6>, 2020.

839 Zhou, J., Yang, K., Crow, W.T., Dong, J., Zhao, L., Feng, H., Zou, M., Lu, H., Tang, R. and Jiang, Y.:  
840 Potential of remote sensing surface temperature-and evapotranspiration-based land-atmosphere  
841 coupling metrics for land surface model calibration, *Remote Sensing of Environment*, 291, 113557,  
842 <https://doi.org/10.1016/j.rse.2023.113557>, 2023.



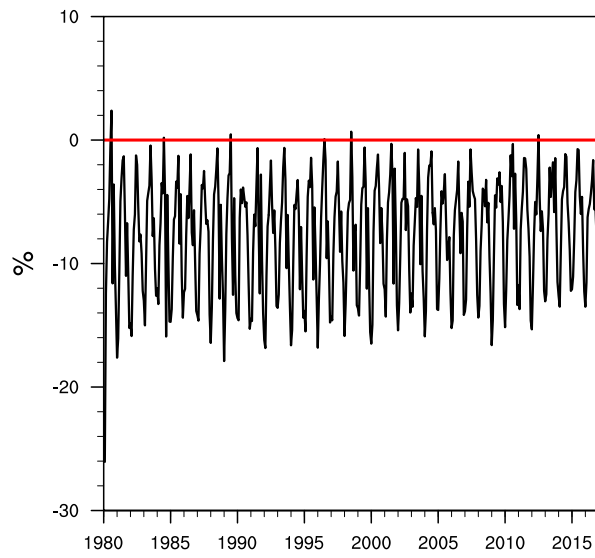
843  
844  
845

**Figure 1.** Flowchart of the 4DEnVar-based WCLDA system in E3SMv2 based on the DRP-4DVar method.



846

847 **Figure 2.** Schematic flowchart of the 4DVar-based WCLDA system. The beginning of a month is at  
 848 0000 UTC on the first day of the month, and the end of the month is at 0000 UTC on the first day of the  
 849 next month.  $x_b$  denotes the background vector including the backgrounds of all E3SMv2 components  
 850 (atmosphere ( $x_b^{atm}$ ), ocean ( $x_b^{ocn}$ ), sea ice ( $x_b^{ice}$ ), river transport ( $x_b^{river}$ ) and land surface ( $x_b^{lnd}$ )).  $x_a$   
 851 consists of the assimilation analysis of land surface ( $x_a^{lnd}$ ) and the backgrounds of other components.  
 852  $y_b^{lnd}$  represents the simulated monthly mean soil temperature ( $T_b^m$ ) and moisture ( $M_b^m$ ) by E3SMv2 using  
 853  $x_b$  as the initial condition.  $y_{obs}^{lnd}$  denotes the monthly mean GLDAS data of soil temperature ( $T_{obs}^m$ ) and  
 854 moisture ( $M_{obs}^m$ ).  $y'_{obs}$  denotes the observational innovation, which is the difference between the GLDAS  
 855 data ( $y_{obs}^{lnd}$ ) and the observational background ( $y_b^{lnd}$ ).

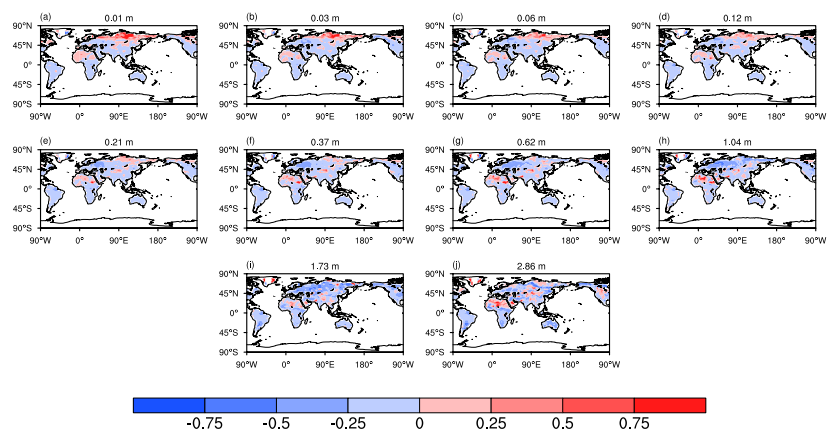


856

857 **Figure 3.** Time series of the reduction rate of the cost function from 1980 to 2016 in the 4DnVar-based

858 WCLDA system.

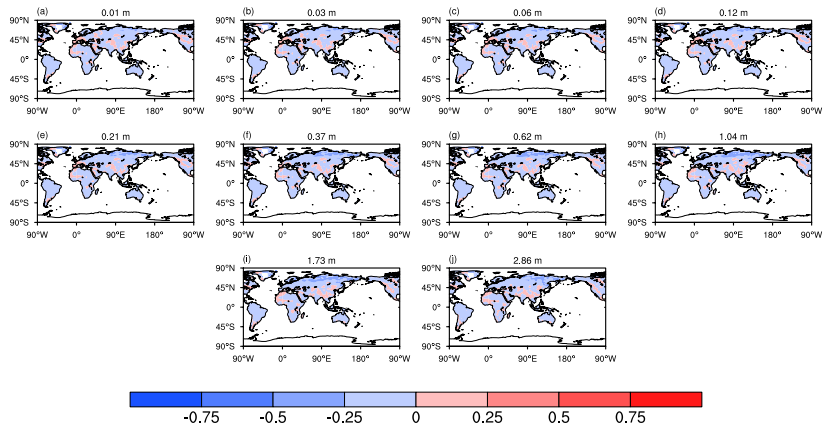




859

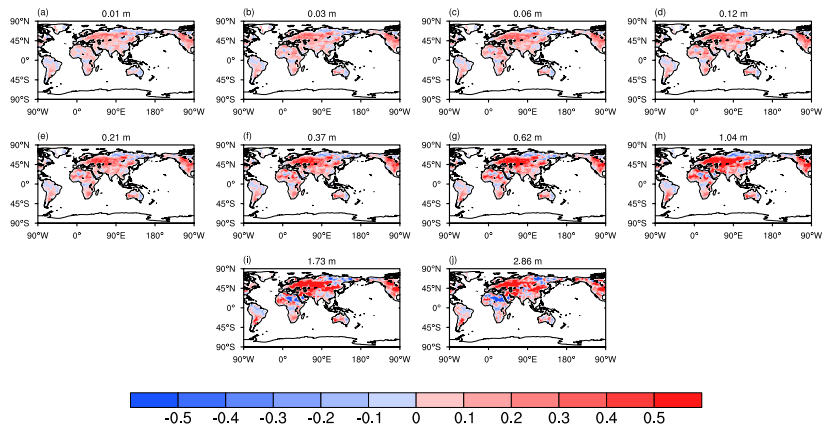
860 **Figure 4.** Spatial distribution of the AE index for soil moisture from the surface to deep layers during

861 the 1980-2016 period. The number at the top center denotes the depth of each soil layer.



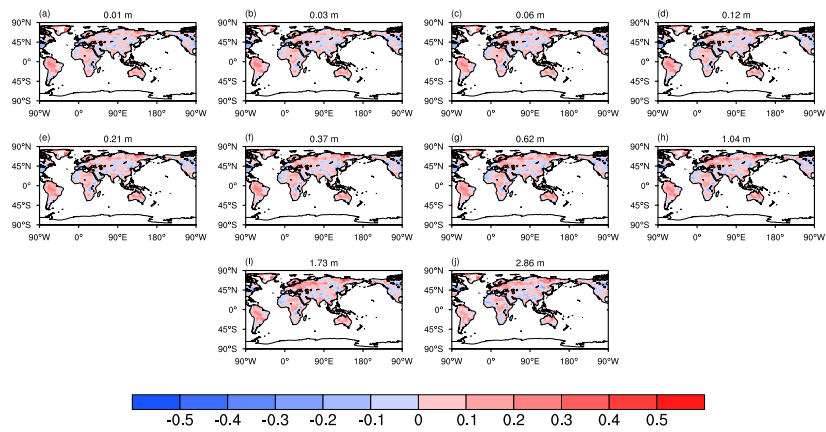
862

863 **Figure 5.** Same as in Figure 4, but for soil temperature.



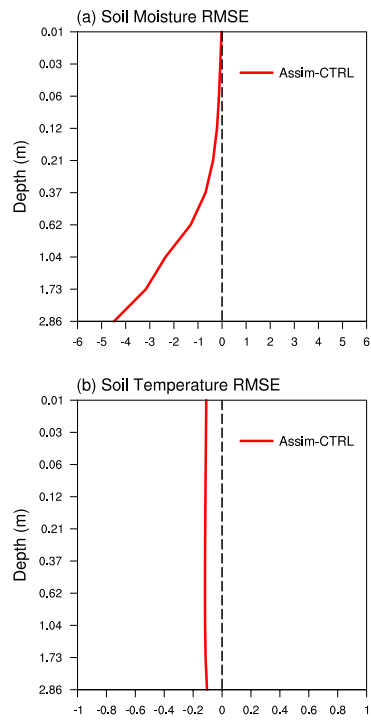
864

865 **Figure 6.** Differences between correlations of soil moisture in Assim and CTRL with the GLDAS data  
 866 from the surface to deep layers for the period of 1980-2016. The number at the top center denotes the  
 867 depth of each soil layer.



868

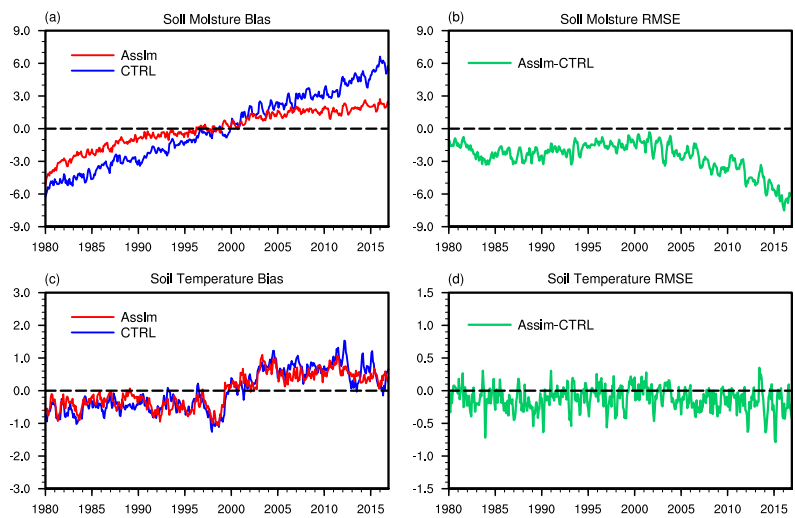
869 **Figure 7.** Same as in Figure 6, but for soil temperature.



870

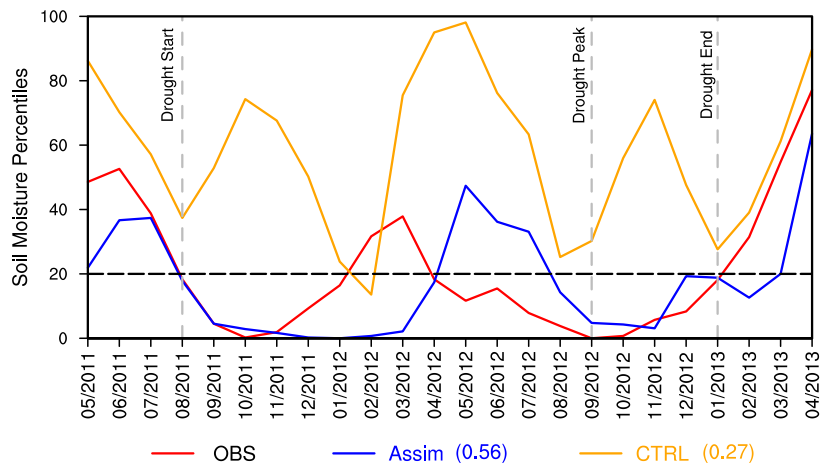
871 **Figure 8.** Vertical distributions of RMSE differences (Assim minus CTRL) for (a) soil moisture and (b)

872 soil temperature averaged over the global land during the 1980-2016 period.



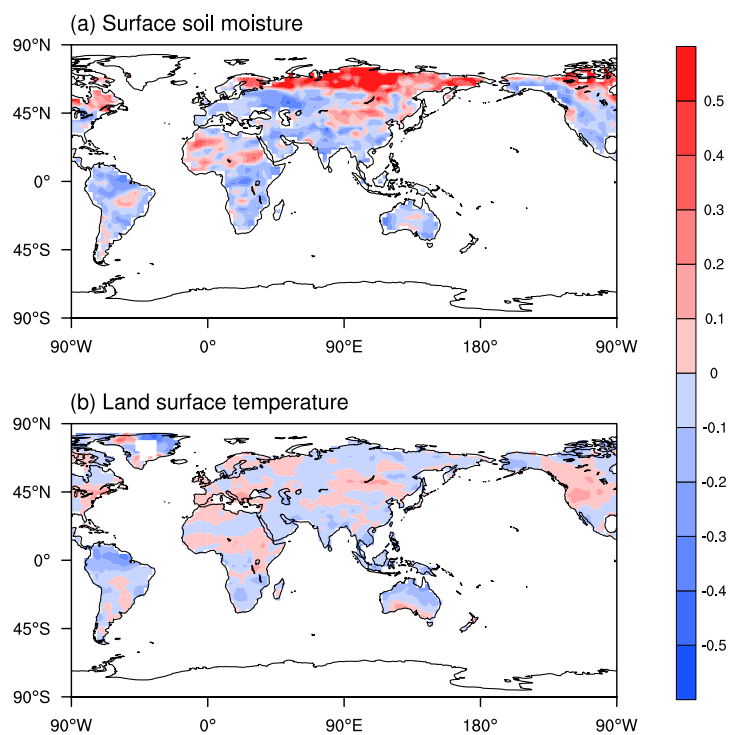
873

874 **Figure 9.** Time series of the vertically averaged global mean soil moisture and temperature bias (left) for  
 875 Assim (red line) and CTRL (blue line), and RMSE differences (right, green line) between Assim and  
 876 CTRL from 1980 to 2016.



877

878 **Figure 10.** Time series of soil moisture percentiles between May 2011 and April 2013 during the 2012  
 879 U.S. Midwest drought. Red line: observation, blue line: Assim, orange line: CTRL. The correlation  
 880 coefficients of Assim and CTRL with observations are also shown. The three vertical dashed lines mark  
 881 the timing of drought start, drought peak and drought end, respectively. The start of the agricultural  
 882 drought is defined as the month when soil moisture falls below the 20th percentile. The soil moisture  
 883 percentiles are averaged over the U.S. Midwest (36°-50°N, 102°-88°W). The observed soil moisture is  
 884 derived from ERA-Interim monthly soil moisture data.



886

887 **Figure A1.** Spatial distribution of the AE index for (a) surface soil moisture and (b) land surface  
888 temperature during the 2003-2014 period. The surface soil moisture and land surface temperature are  
889 derived from monthly AMSR and MODIS satellite data, respectively.